Construction and Building Materials 263 (2020) 120115

Contents lists available at ScienceDirect

Construction and Building Materials

journal homepage: www.elsevier.com/locate/conbuildmat

Experimental and numerical investigations of reinforced concrete columns confined internally with biaxial geogrids

Anas Daou [a], Ghassan Chehab [a], George Saad [a], Bilal Hamad [b,*]

[a] Department of Civil and Environmental Engineering, American University of Beirut, Beirut, Lebanon
[b] Department of Civil and Environmental Engineering, American University of Beirut, P.O. Box 11-0236 Riad El Solh, 1107-2020 Beirut, Lebanon

HIGHLIGHTS

- The objective was to get a better understanding of geogrid-confined R/C columns.
- Experimental and analytical investigations of small-scale columns were conducted.
- Specimens were internally confined with stirrups or biaxial geogrids.
- Results showed that internal confinement by biaxial geogrids enhances ductility.
- Moreover, such confinement increases energy absorption capacity.

ARTICLE INFO

Article history:
Received 6 March 2020
Received in revised form 26 June 2020
Accepted 30 June 2020
Available online 20 July 2020

Keywords:
Concrete columns
Ductility
Confined concrete
Biaxial geogrids
Stirrups

ABSTRACT

Geogrids are geosynthetic materials that have been proven effective for stabilization and strengthening applications in infrastructure, such as: reinforcement and stabilization of pavement layers, reinforcement of embankments and soil walls, in addition to soil improvement. The main aim of this study is to investigate the feasibility of using biaxial geogrids as a replacement of ordinary transverse steel reinforcement in columns. Using geogrids as confining material in reinforced concrete columns offers advantages over steel stirrups in that they are less laborious to install and are more durable. The study presents results of experimental and analytical investigations of the behavior of small-scale reinforced concrete columns of 500 mm height subjected to monotonic uniaxial compressive loading. The main test variables include confining material (steel stirrups or geogrids), number of geogrids layers, and the aspect ratio (height to diameter) of the column. Strain gauges were installed on the geogrids to determine the displacement fields of the geogrid elements. Axial displacement and axial load were measured to assess the overall load-displacement behavior, stiffness, ultimate strength, and ductility of the confined column specimens. Analysis of the results revealed that the ductility and energy absorption capacity of concrete column specimens are substantially enhanced without any significant effect on the ultimate load capacity when internally confined by biaxial geogrids. Two distinct analytical models were developed to predict the load-displacement behavior, one for unconfined plain concrete specimens, and the other for columns with transverse reinforcement using biaxial geogrids. The models provided satisfactory predictions of the stress–strain response when the analytical and experimental results were compared.

1. Introduction

Reinforced concrete columns are considered among those structural elements that are most vulnerable for failure under dynamic and impact loading due to earthquakes or blast loads. Failure of columns often leads to catastrophic collapse of the structure they are incorporated. Thus, ensuring that columns and other associated structural elements in reinforced concrete (R/C) buildings exhibit ductile behavior is of paramount importance. As such, numerous research has been conducted to evaluate the effects of incorporation and configuration of stirrups, and various types of fibers on flexural and shear strength of R/C members. Additionally, extensive research has been conducted on the development and improvement of innovative and smart materials that are characterized by high strength, light weight and increased ductility to reduce inertial forces and cost, and improve durability. This study focuses on the use of geogrids, a geosynthetic material, that is

* Corresponding author.
E-mail address: bhamad@aub.edu.lb (B. Hamad).

https://doi.org/10.1016/j.conbuildmat.2020.120115
0950-0618/

starting to gain popularity in the construction industry, particularly in the infrastructure sector. Various research studies have revealed significant benefits and high potential in adopting geogrids for various novel applications in construction. Most of such research work has revolved around the use of geogrids for transportation infrastructure applications, geotechnical applications, and structural foundations [1,5,14,15,18,20,21]; whereas, very little effort has been exerted and documented on the use of geogrids as alternative transverse reinforcement in R/C columns.

Adding geogrids in R/C columns is a technique where tensile elements (geogrids) are placed internally inside the periphery of the concrete column to improve stability and reduce transverse deformation. Geogrids are tied to the vertical reinforcement within the concrete column before casting to serve as a sturdy confining medium in the columns. The tensile capacity of the geogrids can be used effectively as they can be formed into a circular shape without sharp bends. Placing internal geogrid layers provides tensile resistance upon expansion of the loaded columns and inhibit propagation of cracks through its ribs serve the same contribution as the steel stirrups do, with the advantage of being more ductile Additionally, providing internal confining geogrids which feature high durability and no corrosion susceptibility leads to the possible reduction of the concrete cover thickness.

2. Literature review

Geogrids are classified as geosynthetic materials featuring a grid structure with various aperture sizes. Most common geogrids comprise either of woven textile or of extruded polypropylene. The comprising materials, physical properties, and mechanical properties vary depending on the specific needs of the application in question. Classifying geogrids as uniaxial, biaxial, or triaxial depends on the number of directions in which the ribs extend and consequently the directions they reinforce. Each of these types could either be woven or punched-drawn non-woven based on their mechanical and physical properties as well as their process of manufacture. Given a proper ratio of geogrid aperture size to aggregate grain size, geogrids provide effective lateral confinement in media that comprise of unbound and bound aggregates.

Though commonly used in soils, geogrids are less used in concrete. Therefore, more efforts are currently put into investigating the possibility of using geogrids to reinforce Portland Cement Concrete (PCC) structural members to benefit from their tensile strength and ductility. The results from most studies were very promising in that regard, as concrete gains both early and post-cracking ductility and load capacity.

2.1. Previous applications on geogrids use in concrete

In an experimental study, Al-Ayash et al. [4], assessed possible advantages to using geogrids as a confinement tool in PCC cylinders taking into consideration different types of geogrids and different number of reinforcement layers (one layer and two layers). One point to consider is that the tensile strength of biaxial geogrids (BG) is lower than that of the uniaxial ones. Plain concrete cylinders exhibited brittle failure. Cylinders confined with two layers of uniaxial geogrid (UG) hoops showed the highest ductility after initial cracking of concrete. Cylinders confined with one layer of uniaxial geogrids and those confined with one layer of biaxial geogrids behaved similarly to cylinders confined with steel hoops in the stage of post-cracking. In addition, cylinders confined with one layer of biaxial geogrids were found to have the highest ultimate axial load which indicated that the mesh shape of the biaxial geogrids is a factor that resulted in additional compressive strength rather than the geogrid's tensile strength noting that the tensile strength of biaxial geogrids is relatively lower than that of the uniaxial type.

Moreover, in a study by El Meski and Chehab [11], triaxial, biaxial and uniaxial geogrids with various properties, mechanical and physical, were used to reinforce nine ordinary strength concrete beams and six high strength concrete beams. The samples were exposed to four-point monotonic load bending until failure. When the results of geogrid-reinforced beams load-deflection were compared to those of plain concrete, the deflection of all geogrid-reinforced samples was larger by far which can be interpreted as a very ductile post-cracking behavior as compared to the plain concrete specimens' brittle failure. The initial crack appeared earlier for geogrid-reinforced members due to the weaker concrete section separated by the geogrid sheet. However, in the post-cracking stage, cracks increased gradually as the geogrids resisted the load until they failed.

In addition, laboratory study by Tang et al. [25] assessed how members of geogrid-reinforced PCC behaved through comparing the effects of utilizing one or two layers of flexible and stiff biaxial geogrids. Moreover, when using geogrid reinforcement, similar benefits could be noticed with regards to improved energy absorption capacity and load capacity as well as post-cracking ductility. When compared to flexible geogrids, stiff geogrids yielded higher benefits which confirms that geogrids' mechanical and physical properties play an essential role in the concrete reinforcement efficiency. Finally, introducing a second geogrid layer caused a significant increase in post-cracking ductility and load capacity which peaked at around 60% of the maximum load that caused the first crack.

Sivakamasundari et al. [24] studied the effectiveness of utilizing biaxial geogrids as shear reinforcement along with steel fibers. The study considered the following three types of samples and compared their tensile and compressive behavior: a control cylinder made of plain concrete, a confined one with a tubular shaped biaxial geogrid, and a third one similar to the second but adding steel fibers. The results showed that using geogrid confinement with steel fibers increased the specimens' tensile and compressive strength. Other concrete beams with various shear reinforcement techniques were also tested under three-point monotonic loading: a control beam transversally reinforced with steel stirrups only, a second beam containing in addition to the steel stirrups biaxial geogrid-transverse reinforcement in the hinge region, and a third one with a certain amount of steel fibers along with steel stirrups and geogrids. The study concluded that when compared with using geogrids alone, the use of geogrids for transverse reinforcement along with steel fibers showed a massively improved post cracking behavior as well as energy dissipation capacity of the beams.

Al-Hedad et al. [3] investigated how the use of geogrids affects concrete pavements with drying shrinkage behavior. Two types of specimens were prepared and cured for one week, after which they were stored in a drying room for fifty-six days. As for the first type, it consisted of concrete prisms, of 75 mm thickness, among which some specimens were control and others contained one sheet of biaxial geogrids placed at one of two different locations from the top (20 or 37.5 mm). Test results showed that after 14 days, geogrid reinforcements were able to reduce the drying shrinkage strains by 0.7 to 15% compared with unreinforced prisms. However, geogrid sheets placed at 20 mm from the top were more effective during the early stage than those placed at 37.5 mm in terms of reducing drying shrinkage strains. After 21 days, both groups (placed at 20 and 37.5 mm) had approximately the same effect. The second type of specimens included concrete slabs, of 30 mm thickness, among which some specimens were plain concrete and the others reinforced by placing at 15 mm from the top one sheet of biaxial geogrids. When compared with plain concrete slabs, the drying shrinkage strains were reduced between 7 and 28%.

The confinement effects of geogrid and steel fibers on the mechanical properties of concrete specimens under compression and flexure were investigated by Chidambaram and Agarwal [7]. An experimental program on concrete specimens was organized. Test specimens comprised of concrete cylindrical specimens and flexural tests on R/C beams. Results showed that geogrid could be used as an effective alternative material to confine the concrete as compared to conventional techniques. Using the combination of geogrid and steel fiber reinforced concrete (SFRC) was found to have a significant improvement of the stress–strain behavior of the concrete specimens. Also, the positive effect of geogrid confinement with and without steel fibers for cylindrical specimens under split tension was indicated. Tests on flexural beams revealed the importance of the number of geogrid layers and its strength in improving the load-deformation behavior and crack propagation where geogrid provided an effective crack bridging mechanism.

Furthermore, Chidambaram and Agarwal [8] investigated the performance of beam-column joint specimens using conventional confinement and geogrid confinement with and without SFRC under cyclic loading. The load-deformation curves, energy dissipation, strength and stiffness degradation, moment rotation relationships, and failure pattern with specified damage index were compared to verify the efficacy of the test results. It was found that joint performance was significantly improved by using geogrid confinement, and that shear strength of the joint was further increased by the use of SFRC.

More experimental studies were reported by Chidambaram and Agarwal [9]. The purpose of the work was to examine the feasibility of geogrid confinement as additional shear reinforcement in R/C beams, and the combined effect of geogrid confined R/C beams with SFRC under flexure and shear. The test program consisted of twelve sets of beams which were divided into three types with different configurations. The main variables were the ratio of longitudinal and transverse reinforcement, the strength of geogrid, and the volume of steel fibers. It was found that geogrid confinement enhanced the stiffness degradation and energy dissipation property, and the composite action of the proper application of geogrid confinement with SFRC helped to achieve ductile behavior and to alter the failure modes. The increase in the strength and post-yield behavior of the beams depended on the volume percentage of the fibers and the amount of geogrid confinement.

Geogrid confinement material was also used in R/C elements to study the shear resistance behavior under static and cyclic loading by Chidambaram and Agarwal [10]. Six types of R/C beams and four beam-column specimens with modified stirrups ratio and geogrid confinement were tested. The main aim of the study was to examine the effect of geogrid confinement on the shear resistance capacity with different stirrups spacing. The composite action of steel fibers with minimum percentage and geogrid confinement with increased stirrups spacing, was considered to study the improvement of the shear capacity and the inelastic behavior of R/C beams. The performance of the tested beams was evaluated through the load deformation curves, post-elastic strength and stiffness degradation, energy dissipation, and failure patterns. It was concluded that the shear capacity was improved with better inelastic response when geogrid materials were added to the R/C elements. In addition, improved energy dissipation and better crack distribution of the composite action provided by the geogrid and minimum percentage of steel fibers in R/C beams and beam-column elements were obtained.

The effects of polyester geogrids used as a shear reinforcement bar for corroded and uncorroded R/C beams were investigated by Yalciner et al. [27]. Ten R/C beams were tested using two different configurations of shear reinforcement (ordinary stirrups and geogrid). The test beams were subjected to an accelerated corrosion method using six different corrosion levels: 0%, 2, 3, 5, 6 and 9%. The geogrid confinement beams were compared with the conventional R/C beams for each corrosion level. The effects of the geogrid on the characteristic properties (flexural strength, moment–curvature, bond slip, and crack pattern) were assessed. It was concluded that performance of the geogrid was very poor when compared to conventional beams with ordinary stirrups, and hence the use of geogrid as shear reinforcing bars in R/C beams at the considered levels of corrosion was found unsatisfactory.

2.2. Previous research on confinement of concrete columns

Priestly et al. [23] used fiber reinforced polymer (FRP) material in concrete columns. It was found that using external FRP confinement could significantly increase the concrete strength and ductility. One method of confinement is wrapping FRP sheets around the concrete column. To provide confinement for the concrete, the sheets are bonded to the concrete column's exterior surface and oriented in the direction of the hoop. Many experimental research studies, such as those reported by Fam and Rizkalla [12], Lam and Teng [16], Li and Hadi [17], as well as Hadi [13], have been conducted in this area.

Lam and Teng [16] conducted an overall assessment and review of available models. The proposed FRP confined concrete stress–strain models can be either "design-oriented" or "analysis-oriented". In the design-oriented models, evaluation of experimental data is done to create the stress–strain curve. As for the analysis-oriented models, generating the stress–strain curve is possible by considering the interaction between the confining FRP and the concrete core. The confined concrete compression strength and its strain were calculated at the point of yield of transverse steel and expressed as function of the effective lateral confining pressure f_l. A database consisting of seventy-six specimens confined with carbon, glass or aramid FRP were used. Findings based on the analysis oriented model showed that when the confinement ratio β, defined as the ratio of the effective lateral confining pressure f_l to the axial concrete compressive strength f'_{c0}, was larger than 0.07, an ascending post-peak branch was expected leading to a considerable strength enhancement. For the cases of confined specimens with a confinement ratio less than 0.07, no considerable strength enhancement was assumed and a stress–strain curve with a descending post-peak branch was expected.

3. Research significance and scope

Very few studies are documented in the literature on the effectiveness of geogrids in providing confinement of concrete columns. Additionally, structural design codes, specifications and standards do not address geogrid-confined columns. This gap, however, needs to be filled through a number of well-controlled experimental, analytical, as well as numerical research studies. Compared with other materials, geogrids have a number of advantages such as: corrosion resistance, light-weight, low cost, commercial availability, ease of construction, and sustainability. All these features are of utmost importance in structural applications.

The research conducted in this paper is essential for a better understanding of the structural behavior of geogrid-confined R/C columns. The study, conducted at the Material and Structural Engineering Laboratory of the American University of Beirut, investigated the behavior of biaxial geogrid-confined circular concrete columns subjected to concentric monotonic axial compressive stress. The major objective was to evaluate as well as quantify the level of effectiveness of using biaxial geogrids (BG) in Portland cement concrete (PCC) columns as an alternative to the conventional transverse reinforcement. To better understand the mechanism by which geogrid confinement influences the behavior of circular R/C columns, several behavioral aspects were evaluated including the axial load capacity and deflection response, the mode of failure, and the accumulated energy. Effects of several design parameters were considered including the type of internal transverse reinforcement, the number of layers of internal geogrid confinement, and the diameter to height (D/H) ratio of the column sections. To predict the BG confined concrete axial compressive behavior, analytical and numerical models were also developed.

4. Experimental program

4.1. Test specimens and parameters

Fourteen small-scale column specimens with a height ranging from 450 to 600 mm and a diameter of 230 mm were subjected to axial monotonic compressive stress. Some specimen replicates were used to verify the experimental test results. The main test variables included the confining material (stirrups or biaxial geogrids), number of geogrid layers, and diameter to height ratio (D/L) of column specimens. One type of geogrid confinement and five different D/L ratios were considered. Depending on the longitudinal steel cage confining material, the specimens were divided into three series (C, S, and BG). The term C represents the column specimen with no confinement, the term S represents columns with transverse steel hoops as confining material; whereas, the term BG represents columns with biaxial geogrids as confining material. Table 1 summarizes the designations, sizes and corresponding test parameters of the specimens. The number following BG corresponds to column height (cm); 1L implies one geogrid layer whereas 2 L implies two layers. The number following S (5, 10, 15, or 20) corresponds to spacing of the stirrups in cm. For example, specimen BG-50-1L is a 50 cm long column specimen with one layer of biaxial geogrid confinement. Specimen S-50–5 is a 50 cm long column specimen with 5 cm stirrups spacing.

4.2. Testing and materials

4.2.1. Concrete material

All specimens were cast using a single batch of Ready-Mix (R/M) concrete. The concrete material consisted of Portland cement Type I, sand, and well-graded coarse aggregate with a maximum size of 9.5 mm. The mix design proportions are determined in accordance with the ACI 211.1-91 [2]. The water-cement ratio was controlled to produce an intended concrete compressive strength of 11 MPa only, due to the axial testing machine limited capacity. Standard 150 × 300 mm cylinders were cast and tested to calculate the concrete compressive strength. The average concrete compressive strength values at 7 and 28 days were 9 and 11 MPa, respectively.

4.2.2. Geogrids

Geogrids mechanical and physical characteristics significantly affect the effectiveness of the confining mechanism. Tang et al. [25] noted that performance of geogrids is impacted by their mechanical and physical properties. Biaxial geogrids (BG) comprise two-directional slim ribs attached at denser joints, thus providing ductile support transversally and longitudinally. In this study, the geogrids were punched-drawn non-woven stiff geogrids consisting of high density polypropylene. Table 2 details the mechanical and physical characteristics of the geogrids from the supplier. Fig. 1 shows the biaxial geogrids used in this study. To obtain the needed cylindrical shape, the geogrids sheets were meticulously rolled and fixed in place in the transverse direction around the vertical reinforcing bars with 300 mm overlap between the sheet's ends for both the one and two layered confined specimens. Because the geogrids were relatively stiff, 150 mm was the minimum diameter that could be obtained. Thus, fabricating columns with smaller diameters in an attempt to study slender columns was not possible, especially given the specimen height limitation dictated by the testing machine in the lab.

To determine the geogrids tensile properties, several geogrid strands were tested using a servo-hydraulic universal testing machine. The total length of the biaxial geogrid strand was 150 mm with a free length of 100 mm. The displacement-controlled test was carried out at a rate of 3 mm/min. The average ultimate tensile load was approximately 1.21 kN, with a resulting strength of 233 MPa and with an elastic modulus of 81 GPa. The stress–strain behavior of the biaxial geogrids is shown in Fig. 2.

Table 2
Physical and mechanical properties of the biaxial geogrids (BG).

Property	Unit	Value
Load at 2% strain	kN/m	14
Load at 5% strain	kN/m	28
Ultimate Tensile Strength (L/T)	kN/m	40/40
Opening size (L/T)	mm/mm	33/33
Rib width (L/T)	mm/mm	2.2/2.5
Rib thickness (L/T)	mm/mm	2.2/1.4
Junction thickness	mm	5.8

Note : L = Longitudinal direction, T = Transverse direction.

Table 1
Test specimens.

SpecimenID	Geometry					Material			
	D (mm)	L (mm)	D/L	r** (mm)	Slenderness ratio*** kL/r	f'_c (MPa)	Type of confinement	Spacing of stirrups (mm)	Number of geogrid layers
C*	230	500	0.46	57.50	8.695	11	none	–	–
BG-50-1L*	230	500	0.46	57.50	8.695	11	Biaxial geogrids	–	1
BG-50-2L*	230	500	0.46	57.50	8.695	11	Biaxial geogrids	–	2
BG-40-1L	230	400	0.58	57.50	6.956	11	Biaxial geogrids	–	1
BG-45-1L	230	450	0.51	57.50	7.826	11	Biaxial geogrids	–	1
BG-55-1L	230	550	0.42	57.50	9.565	11	Biaxial geogrids	–	1
BG-60-1L	230	600	0.38	57.50	10.434	11	Biaxial geogrids	–	1
S-50-5	230	500	0.46	57.50	8.695	11	Stirrups	50	–
S-50-10*	230	500	0.46	57.50	8.695	11	Stirrups	100	–
S-50-15	230	500	0.46	57.50	8.695	11	Stirrups	150	–
S-50-20	230	500	0.46	57.50	8.695	11	Stirrups	200	–

*Two replicates for this specimen were tested to validate the test results.
**r = 0.25 D is the radius of gyration.
***(kL/r) is the slenderness ratio; k is the effective length factor = 1.

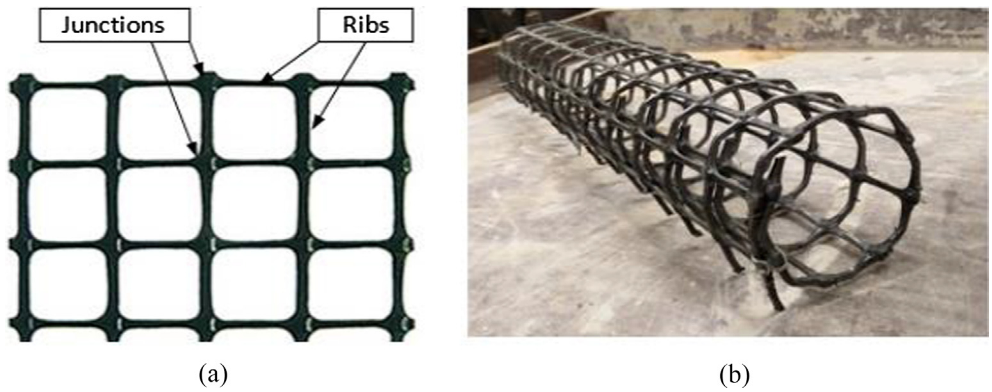

Fig. 1. Biaxial Geogrids: (a) Geogrid plane layer (b) Geogrid cylindrical layer.

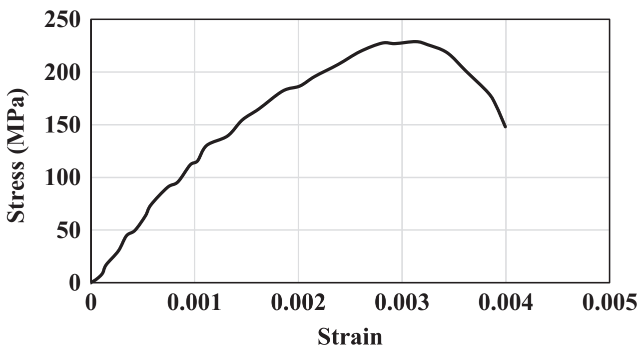

Fig. 2. A typical stress–strain curve of the biaxial geogrids (BG).

4.2.3. Reinforcing steel

The steel reinforcement in the reinforced concrete column specimens comprised four 10 mm Grade 60 deformed longitudinal bars. The transverse ties used were 6 mm Grade 40 plain bars. The spacing of the ties was 50, 100, 150 or 200 mm. Clear concrete cover on all sides of the longitudinal reinforcement was kept constant at 20 mm for all column specimens. The longitudinal bars (Grade 60) yield stress and corresponding ultimate stress were 420 and 560 MPa, respectively, and those of the transverse ties (Grade 40) were 275 and 360 MPa, respectively.

4.2.4. Formwork setup and preparation of specimens

An electric vibrator was used for consolidation of the concrete with a target slump of 200 mm. After stripping the forms, no honeycombing was observed in all specimens. All specimens were covered with wet burlap after casting to maintain them in a moist condition. Specimens were then removed from the formwork after 14 days of casting and were then covered with wet burlap for another 14 days.

4.2.5. Instrumentations and testing

A universal Tinius Olsen testing machine was used to test the specimens in displacement control. An average displacement rate of 1.0 mm/min was until failure of the specimen. Average axial deformations were measured using four linear variable differential transducers (LVDT) attached to the specimens on either side and positioned over a gage length of 230 mm in the central portion of the specimens. Average axial deformations were also measured over the full height of the specimens (gage length = 500 mm) using one LVDT attached between the actuator head and the specimen support. A computerized data acquisition system was used to monitor all data including LVDT readings and the applied load. Figs. 3 and 4 show typical layouts of instrumentation and test set-up.

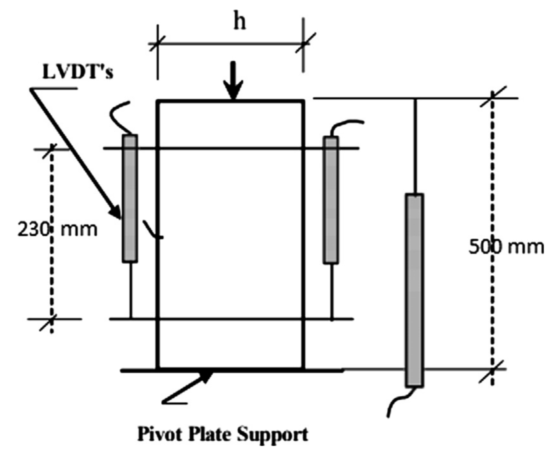

Fig. 3. Typical layout of instrumentations.

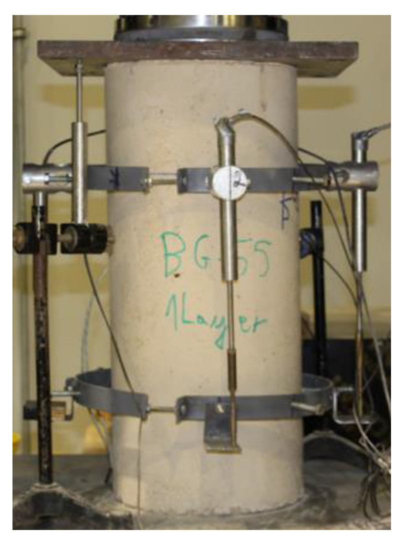

Fig. 4. Test set-up.

5. Testing results and analysis

As the loading was applied to the specimens, signs of damage first appeared as thin longitudinal cracks on the outer surface of the concrete specimen and that then expanded and propagated into the core area accompanied with a series of sharp-pitched sounds resulting from the ruprture of the geogrid junctions. At ultimate failure, the majority of concrete cover had spalled off, the geogrid sheet lost anchorage provided by the overlap, and the sheet wires were ruptured due to the induced high stress concentration developed in the overlap region. Fig. 5 shows typical failure of specimens confined with one-layer geogrids. All geogrid confined concrete specimens showed progressive failure. When the concrete core expanded outwards significantly and the polymer grid rupture was significant, failure occurred. The load carrying capacity for all BG confined concrete specimens was completely exhausted at the end of the test (BG rupture at the junctions), which indicates that the specimens could not carry more axial load with a larger axial deformation. It was also observed that 50-cm concrete specimens confined with one layer of biaxial geogrids had less amount of intact core concrete after failure as compared with concrete specimens confined with two layers of geogrids.

Table 3 show test results that include the measured ultimate axial applied load P_{max}, the ratio of the tested specimen ultimate load to that of the control specimen (α), axial deformations δ_y and δ_f, ratio (μ) of axial deformations δ_f to δ_y, fracture energy (F), and the ratio of fracture energies of tested specimen to the control unconfined specimen (K). With reference to the schematic load-displacement Fig. 6, δ_y is the axial displacement corresponding to the yield load P_y at which the load-displacement curve becomes non-linear and δ_f is the axial displacement that corresponds to one-half of the maximum load reached.

Two indicators were used to measure ductility of the load-displacement history in this research. Ductility is defined as the ability of a structural system or element to undergo inelastic deformation without substantial loss in resistance. The ratio of axial deformations (μ) was assumed as a first measure of ductility of the load-displacement behavior and is called the displacement ductility index. Fracture energy in this research is defined as the area under the load-deformation curve up to δ_f, (refer to Fig. 6). The ratio (K) of fracture energy of the tested specimen to that of the control unconfined specimen was considered as a second measure of ductility of the load-displacement behavior and is called the

(a) (b) (c)

Fig. 5. Typical failures: (a) BG-45-1L, (b) BG-50-1L, and (c) BG-60-1L.

Table 3
Test results.

Specimen ID	Ultimate load P_{max} (kN)	Ratio of ultimate loads α**	δ_y*** (mm)	δ_f*** (mm)	Displacement ductility index μ+	Fracture energy F (N-m)	Energy ductility index K++
C*	465.77	1.000	1.073	4.06	3.784	1346.99	1
BG-50-1L*	456.74	0.981	1.139	9.41	8.262	3585.91	2.662
BG-50-2L*	497.69	1.069	0.976	8.16	8.361	3211.52	2.384
BG-40-1L	455.77	0.979	1.316	8.85	6.725	3100.87	2.302
BG-45-1L	452.52	0.972	1.285	11.04	8.591	4167.8	3.094
BG-55-1L	480.74	1.032	1.319	8.88	6.732	3601.33	2.674
BG-60-1L	451.39	0.969	1.319	11.9	9.022	4792.24	3.558
S-50-5	517.16	1.110	0.89	8.44	9.483	3593.97	2.668
S-50-10*	517.04	1.110	0.99	6.79	6.859	2651.95	1.969
S-50-15	493.21	1.059	1.012	5.15	5.089	1899.9	1.410
S-50-20	492.64	1.058	1.001	5.08	5.075	1860.63	1.381

*Two replicates for this specimen were tested to validate the test results.
** α is the ratio of the ultimate load of the tested specimen P_{max} to that of the control specimen C.
*** δ_y and δ_f are defined in Fig. 6.
+ μ is the displacement ductility index and is calculated as the ratio of δ_f to δ_y.
++ K is the energy ductility index and is calculated as the ratio of the fracture energy of the tested specimen divided by that of the control specimen C; fracture energy is defined in Fig. 6.

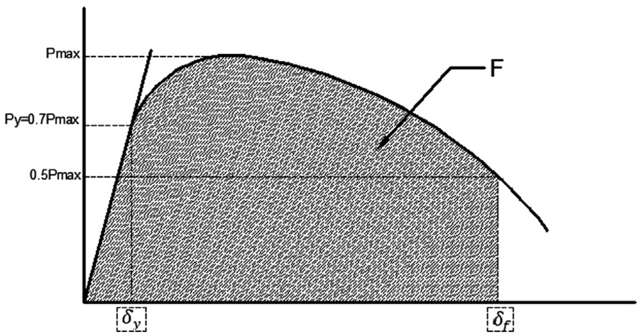

Fig. 6. Schematic of load-displacement curve to define the parameters used in Table 3.

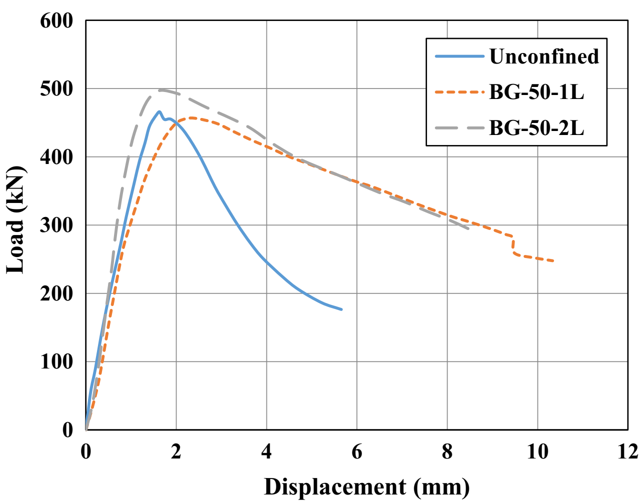

Fig. 7. Effect of number of biaxial geogrid layers on load-displacement history.

energy ductility index. It should be noted that replicate specimens gave very comparable results indicating the validity of the test results.

5.1. Effect of number of geogrid layers

The axial load versus the axial displacement graph of specimens having constant D/L ratio and different number of confining geogrid layers: C (unconfined), BG-50-1L and BG-50-2L is shown in Fig. 7. The load-displacement behavior starts with a linear portion lasting up to approximately 70% of the ultimate load. Thereafter, the curves enter in a nonlinear stage where large strains begin to be registered for small increments of loads. As compared to the maximum load reached by the control specimen with no confinement, the 1-layer BG specimen dropped by around 2%; whereas, the 2-layer BG specimen increased by around 7%. The deformation capacity of the two specimens of BG confined concrete is relatively higher than the unconfined concrete specimen's, as reflected by the value of the displacement ductility index μ (refer to Table 3). Another indication of the positive effect of geogrid confinement on energy absorption is the value of the energy ductility index K

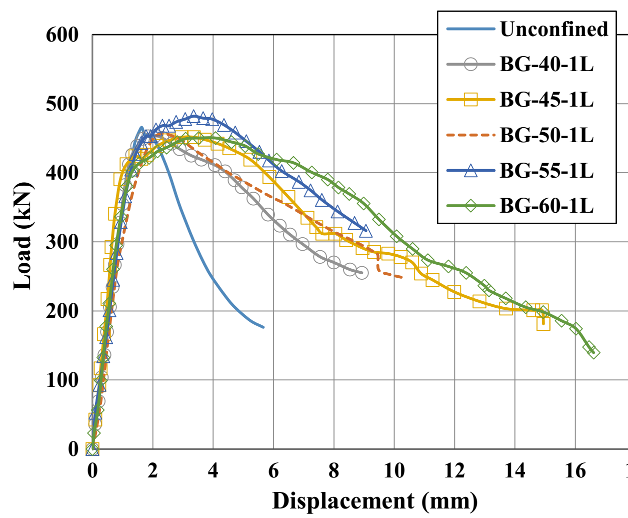

Fig. 9. Effect of diameter to height (D/L) ratio on load-displacement history.

Fig. 8. Failure of specimens with different diameter to height (D/L) ratios.

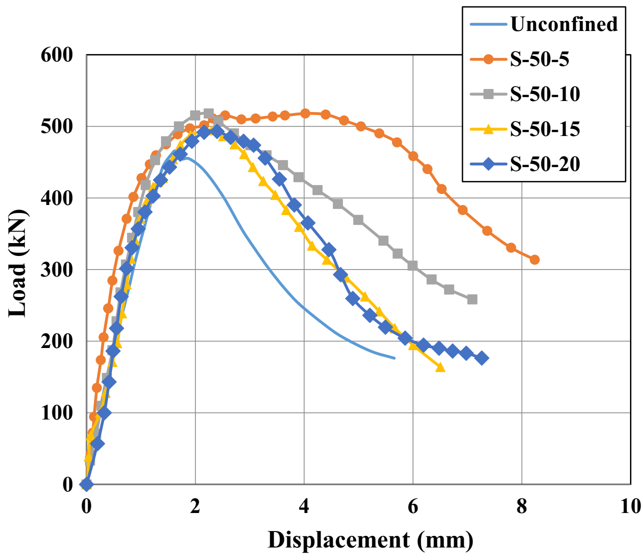

Fig. 10. Effect of stirrups spacing on load-displacement history.

which is 2.662 for the 1-layer BG specimen and 2.384 for the 2-layers BG, as compared to the unconfined concrete specimen C.

5.2. Effect of diameter to height ratio of the tested specimens

The failure modes of the BG confined specimens with different D/L ratios are very similar (refer to Fig. 8). The specimens failed by the formation of a series of cracks in the cover parallel to the axial direction of loading with a loud bursting noise. The concrete's increased hoop deformation implements tensile pressure on the BG sheet which leads to the BG cracking map at a load very close to failure. As the BG sheet ultimate tensile strain was reached, the concrete specimen failed drastically with a sudden explosive release of the stored energy that resulted in the shattering of tiny concrete pieces in all directions. After failure, all the loose concrete pieces from the cover were removed and a typical conical concrete shape appearance was clearly recognized. After examining the delaminated BG sheets, some concrete pieces were still attached to the column core, proving that the bond between the BG sheet and concrete is strong.

The axial load-displacement curves of BG confined concrete specimens with different D/L ratios, presented in Fig. 9, indicate no difference in load-displacement behavior. As compared with the unconfined control specimen C, specimens confined with 1-layer BG and different D/L ratios had ultimate load ratios ranging between 0.969 and 1.032, indicating no significant difference in ultimate load capacity (refer to Table 3). This is the fact that all tested specimens are short columns. However, values of the displacement ductility index μ ranged between 6.725 and 9.022 as compared with 3.784 for the unconfined specimen, and values of the energy ductility index K ranged between 2.302 and 3.558 indicating significant increase in energy absorption of BG confined specimens with different D/L ratios relative to the unconfined specimen C.

5.3. Effect of the stirrups spacing

Fig. 10 shows a plot of the axial compressive load versus the axial displacement of column specimens having constant D/L ratio but with different stirrups spacing. Specimens S-50-20, S-50-15, S-50-10 and S-50-5 had ties spaced at 200, 150, 100 and 50 mm, respectively. Ultimate loads of the 150 and 200 mm tie spacing specimens improved by around 6% relative to the unconfined specimen, whereas the increase was 11% for the 50 and 100 mm spacing (refer to Table 3). The positive effect of stirrup confinement is also indicated by the load-displacement history beyond the ultimate load. Compared to the displacement ductility index of the unconfined specimen C (3.784), the values ranged between 5.075 for the 200-mm stirrup spacing to 9.483 for the 50-mm specimen. The energy ductility index ranged from 1.381 to 2.668.

5.4. Effect of confinement type

In the absence of internal confinement, failure of the concrete specimen was preceded by destruction of the concrete and full

(a) (b) (c)

Fig. 11. Effect of confinement on buckling of longitudinal steel bars (a) C, (b) S-50–15, (c) BG-50-2L.

buckling of the longitudinal steel bars as shown in Fig. 11. The presence of closely spaced stirrups (50 and 100 mm spacing) or geogrid sheets not only provided confinement of the concrete, but also prevented buckling of the steel bars, leading to better performance.

As for the maximum axial load reached, Table 3 listed values indicate that the 1-layer BG specimens recorded slight decreases (with the exception of BG-60-1L) as compared to the control unconfined specimen. However, the 2-layer specimen recorded a 7% increase which is very similar to the 6% increase of the 150 and 200-mm stirrup spacing specimens. The 50 and 100-mm stirrup spacing specimens performed best and recorded an 11% increase in the maximum load.

Load-displacement curves for specimens with different confinement types are shown in Fig. 12. Ductility indexes listed in Table 3 are plotted in Figs. 13 and 14. The two plots clearly indicate that geogrid confinement was more effective in improving the ductility of the load-displacement behavior as compared to the 200 or 150-mm stirrups confined specimens. The 100 and 50-mm stirrup spacing specimens had similar performance as the BG specimens. These results prove that although geogrid confinement could decrease slightly the maximum axial load of the column specimen, however improved ductility due to providing the column core with continuous confinement is significant and is comparable to specimens with very closely spaced stirrups.

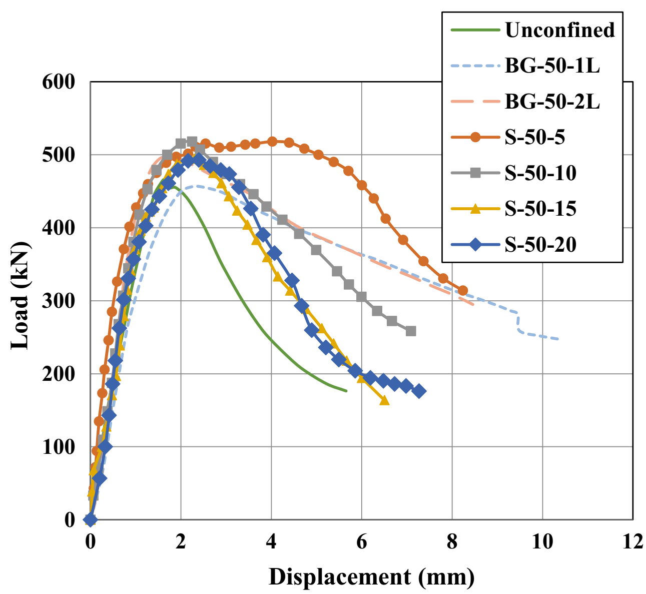

Fig. 12. Effect of confinement type on load-displacement history.

6. Confinement model

There is not enough research in the literature that investigate the development of stress–strain models to predict the axial compressive behavior of Geo-polymer sheets confined concrete. The present study approaches all geogrid reinforced concrete columns that are being designed in highly corrosive environment. Most predictive concrete confinement models in the literature are based on that the confining materials have a constant thickness and fully covers the external surface of the concrete. In the case of geogrids, the cross-ribs cover part of the surface area. The proposed model aims at establishing an equivalency between the spaced geogrid ribs and a uniform thickness membrane that fully wraps the external surface of the concrete. The equivalent thickness of the ribbed geogrid is therefore given by:

$$t_{eq} = \frac{n_l.n_r.b_r.t_r}{h} \quad (1)$$

where: n_l the number of BG layers, n_r is the number of ribs, b_r is the rib's width, t_r is the the rib's thickness and h is the specimen's height. For structural concrete members that have large axial lengths, Eq. (1) becomes:

$$t_{eq} = \frac{n_l.b_r.t_r}{s_r} \quad (2)$$

where: s_r is the BG ribs spacing. To determine the confinement strength (f_u), applying the conditions of equilibrium requires that the force in the confining concrete be equal to the force in the BG core. As a result, the confining strength (f_u) was derived:

$$f_u = \frac{2.t_{eq}}{d_g}.f_{ru} \quad (3)$$

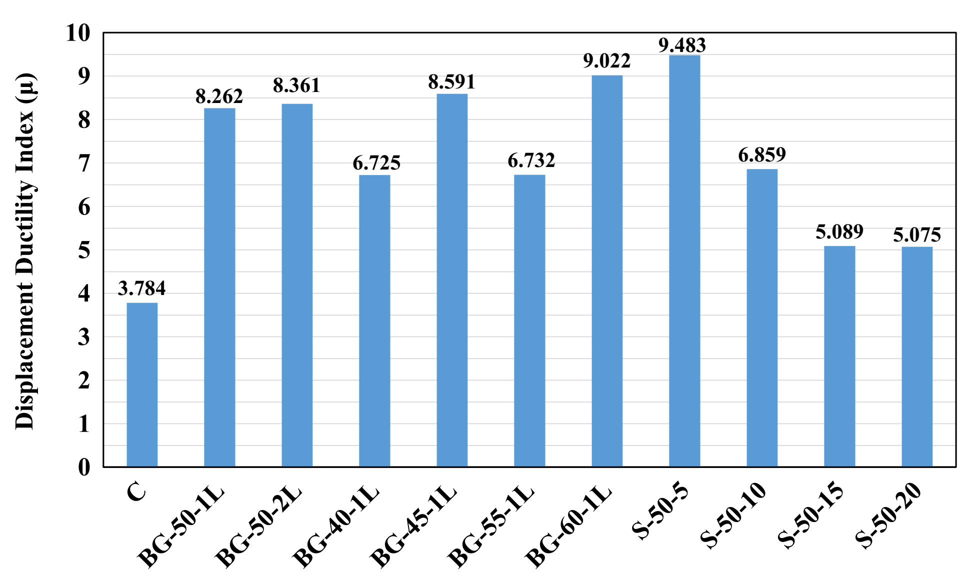

Fig. 13. Variation of Displacement Ductility Index (μ) as measured by the ratio of axial displacements δ_f to δ_y.

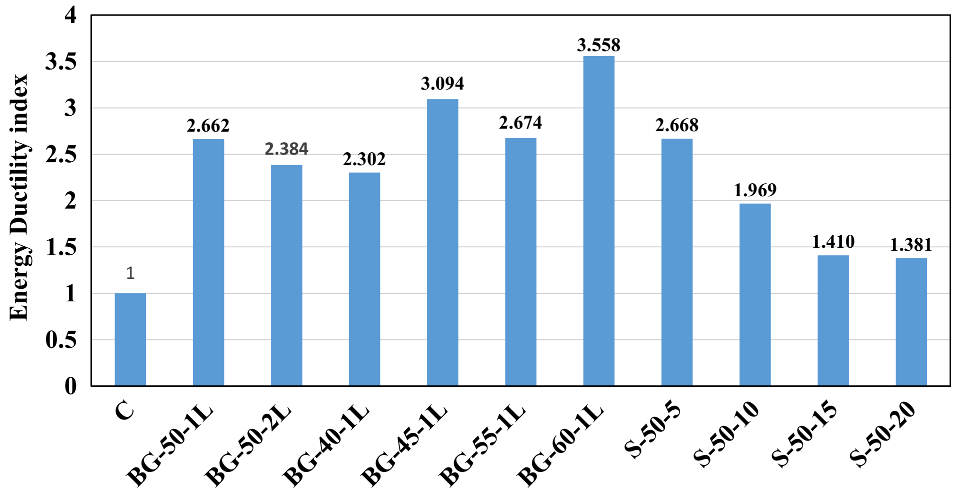

Fig. 14. Variation of Energy Ductility Index (K) as measured by the ratio of fracture energies.

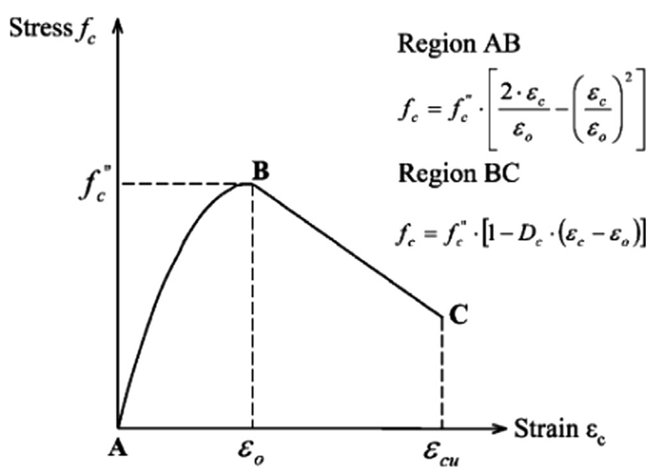

Fig. 15. Modified Hognestad stress strain-curve; Park and Paulay [22].

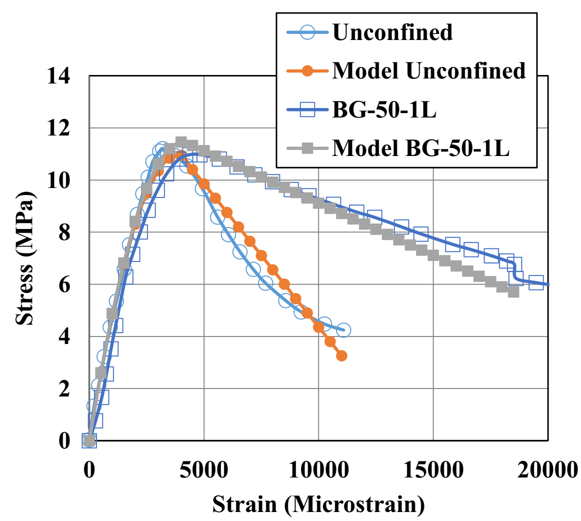

Fig. 16. Experimental and Modified Hognestad Model stress–strain curves of unconfined and 1-layer BG confined specimens.

where f_u is the confinement strength, d_g is the BG sheet diameter and f_{ru} is the BG rib ultimate strength. Considering that the concrete in the column is in a triaxial stress state, the additional confinement strength can be represented by the maximum stress (f''_{cc}) for a cylindrical specimen specified by [19] as:

$$f''_{cc} = f'_c + k_1 f_u \tag{4}$$

where: k_1 is the confinement effectiveness coefficient and is usually assumed between 2.8 and 4.1. It was found that the values of k_1 was overestimated [6] for concrete wrapped with FRP and other confining material. A reasonable value of k_1 was taken as 2 in this study. The axial strain of confined concrete at the peak stress (ε_{co}) was determined using the expression adopted by Wight and MacGregor [26]:

$$\varepsilon_{co} = 1.8 \cdot \frac{f''_{cc}}{E_c} \tag{5}$$

where the secant modulus of elasticity of concrete, E_c, was calculated based on existing empirical expressions:

$$Ec = 4730\sqrt{f'c} \tag{6}$$

and f_c is the minimum specified compressive strength of concrete, in N/mm^2, at 28 days. Eqs. (4) and (5) were combined with the modified Hognestad stress–strain Eq. [22] as follows:

$$f_c = f''_{cc} \cdot \left[\frac{2\cdot\varepsilon_c}{\varepsilon_{co}} - \left(\frac{\varepsilon_c}{\varepsilon_{co}}\right)^2\right] \tag{7}$$

$$f_c = f''_{cc} \cdot [1 - D_c \cdot (\varepsilon_c - \varepsilon_{co})] \tag{8}$$

where ε_c is the concrete strain, ε_{co} is the strain at peak stress of unconfined concrete and ε_{cu} is the ultimate strain. These equations are plotted in Fig. 15. The modified Hognestad equations model the ascending branch (AB, Eq. (7)) with a parabolic relationship and the descending branch (BC, Eq. (8)) with a linearly descending curve. The equation for region BC is based on the deterioration constant (D_c) that controls the slope of the line.

The stress–strain curves of the BG confined concrete were constructed using the material properties of the BG ribs. The following data were considered in the model: A 200 mm BG sheets diameter, the ultimate concrete strain ε_{cu} is 0.015, and data from the tested columns was used to construct the stress strain curve for the BG confined concrete with a deterioration constant was taken equal to 50 that match post peak experimental data. Appendix A shows the detailed implementation of the proposed confinement model. Figs. 16 and 17 present comparisons between the analytical model

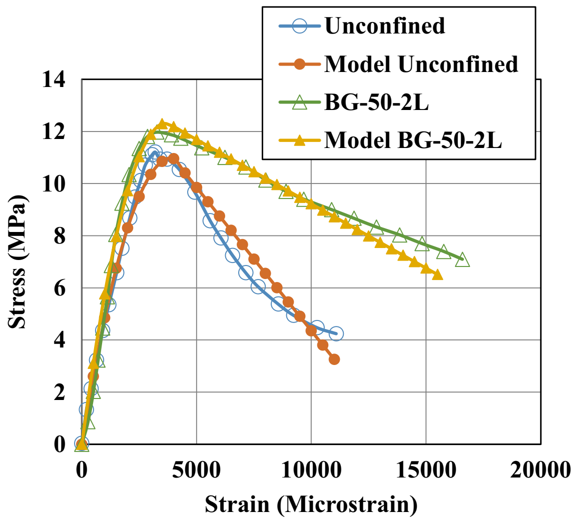

Fig. 17. Experimental and Modified Hognestad Model stress–strain curves of unconfined and 2-layer BG confined specimens.

estimation and the experimental results. The figures show that with the assumed deterioration constant, the modified Hognestad model matches well with the experimental curve.

7. Conclusions

Fourteen small-scale column specimens with constant diameter and varying diameter to height ratios were tested to assess how internal biaxial geogrid confinement affects the maximum axial load and the axial load-axial displacement behavior. Based on the results of the experimental test and the proposed analytical models, the conclusions below could be reached:

a. Internal confinement of the column specimens with 1-layer biaxial geogrids led to slight decrease in axial load capacity. Using two BG layers improved the load capacity by 7%. In comparison, when ties were used to confine the column specimen core, the improvement in axial load capacity was more pronounced especially when small spacings were used.
b. BG internal confinement led to significant improvement in the load-displacement behavior as reflected by the values of the displacement ductility index μ and the energy ductility index K. The displacement ductility index μ which is 8.262 for the 1-layer BG specimen and 8.361 for the 2-layers BG, and that the energy ductility index K which is 2.662 for the 1-layer BG specimen and 2.384 for the 2-layers BG, as compared to the unconfined concrete specimen C. It was noted that the BG internal confinement produces approximately similar improvement caused by small spacing stirrups.
c. No significant difference in ultimate load capacity of specimens with different diameter to height ratios. As compared with the unconfined control specimen, specimens confined with 1-layer BG had ultimate load ratios ranging between 0.969 and 1.032. However, values of the displacement ductility index μ ranged between 6.725 and 9.022 as compared with 3.784 for the unconfined specimen, and values of the energy ductility index K ranged between 2.302 and 3.558 indicating significant increase in the ductility of BG confined specimens with different diameter to height ratios relative to the unconfined specimen.
d. The effect of stirrup confinement was also indicated by the load-displacement history beyond the ultimate load. Values of the displacement ductility index μ ranged between 5.075 for the 200 mm stirrup spacing to 9.483 for the 50 mm stirrup specimen relative to the unconfined specimen.
e. The results showed that geogrid and stirrup confinement do not have significant effect on the ultimate load. However, the improvement of the ductility of the load displacement behavior was indicated. Geogrid confinement was more effective in improving the ductility as compared to the 200 mm and 150 mm stirrups confined specimens. The 100 mm and 50 mm stirrup spacing specimens had similar performance as the BG specimens. The improved ductility of the BG confinement is significant and is comparable to columns with very closely stirrups, and hence geogrid confinement may be considered as a substitute to transverse stirrup confinement.
f. The confinement model proposed by Modified Hognestad stress–strain curve can be applied to geogrids confined concrete columns with appropriate modifications introduced to strength of the geogrids.
g. The analytical model developed for the stress–strain relationship of concrete confined internally with geogrids provided good agreement with experimental data.

Future research needs to be conducted to assess the confinement effect of uniaxial geogrid sheets as compared to biaxial geogrids. Also, it would be significant to compare the effects of internal and external confinement of concrete columns with geogrids.

Declaration of Competing Interest

The authors declare that they have no known competing financial interests or personal relationships that could have appeared to influence the work reported in this paper.

Acknowledgements

The authors highly appreciate the financial support provided by the American University of Beirut. The technical help provided by the staff of the American University of Beirut Civil Engineering laboratory is highly appreciated.

Appendix A

Confinement model – Example

Case: 50 cm long – 1 layer biaxial geogrid confinement

Table A1 below summarizes the properties of the biaxial geogrids used in this study.

number of geogrid layers, n_l = 1

rib width, b_r = 2.2mm

$$rib\ thickenes,\ t_r = 2.2\ mm$$

$$Area\ of\ rib,\ A_b = b_r \times t_r = 4.84\ mm^2$$

$$rib\ spacing,\ s_r = 33\ mm$$

$$number\ of\ ribs\ per\ meter,\ n_r = 30$$

$$diameter\ of\ biazial\ geogrid,\ d_g = 200mm$$

$$height\ of\ specimen,\ h = 50mm$$

Table A1
Physical and Mechanical Properties of the Biaxial Geogrids.

Property	Unit	Value
Load at 2% strain	kN/m	14
Load at 5% strain	kN/m	28
Ultimate Tensile Strength (L/T)	kN/m	40/40
Strain at T_{ult} (L/T)	kN/m	11/10
Opening size (L/T)	mm	33/33
Rib width (L/T)	mm	2.2/2.5
Rib thickness (L/T)	mm	2.2/1.4
Junction thickness	mm	5.8

Note : L = Longitudinal direction; T = Transverse direction.

$$average\ unconfined\ concrete\ stress,\ f_c^{'} = 11Mpa$$

$$Equivalent\ thickness\ of\ uniform\ membrane,\ t_{eq} = \frac{n_l.b_r.t_r}{s_r} = 0.15mm$$

$$geogrid\ ultimate\ strength,\ f_{ru} = \frac{40kN}{m} \times \frac{\frac{1000N}{kN}}{30\frac{ribs}{m} \times \frac{4.84mm^2}{rib}} = 275Mpa$$

$$confinement\ strength,\ f_u = \frac{2.t_{eq}}{d_g}.f_{ru} = 0.4Mpa$$

$$peak\ stress,\ f''_{cc} = f'_c + k_1.f_u = 11 + 2 \times 0.4 = 11.8\ Mpa$$

$$Secant\ Modulus\ of\ Elasticity,\ \text{QUOTEEc} = 4730\sqrt{\text{f}'\text{c}} = 15687\ \text{Mpa}$$

$$\text{axial strain at peak stress},\ \varepsilon_{co} = 1.8 \times \frac{f''_{cc}}{E_c} = 0.00135$$

$$Equation\ for\ Ascending\ Branch\ of\ predictive\ model: f_c = 11.8 \times \left[\frac{2 \cdot \varepsilon_c}{0.00135} - \left(\frac{\varepsilon_c}{0.00135}\right)^2\right]$$

$$Equation\ for\ Dscending\ Branch\ of\ predictive\ model: f_c = 11.8 \times [1 - 50 \cdot (\varepsilon_c - 0.00135)]$$

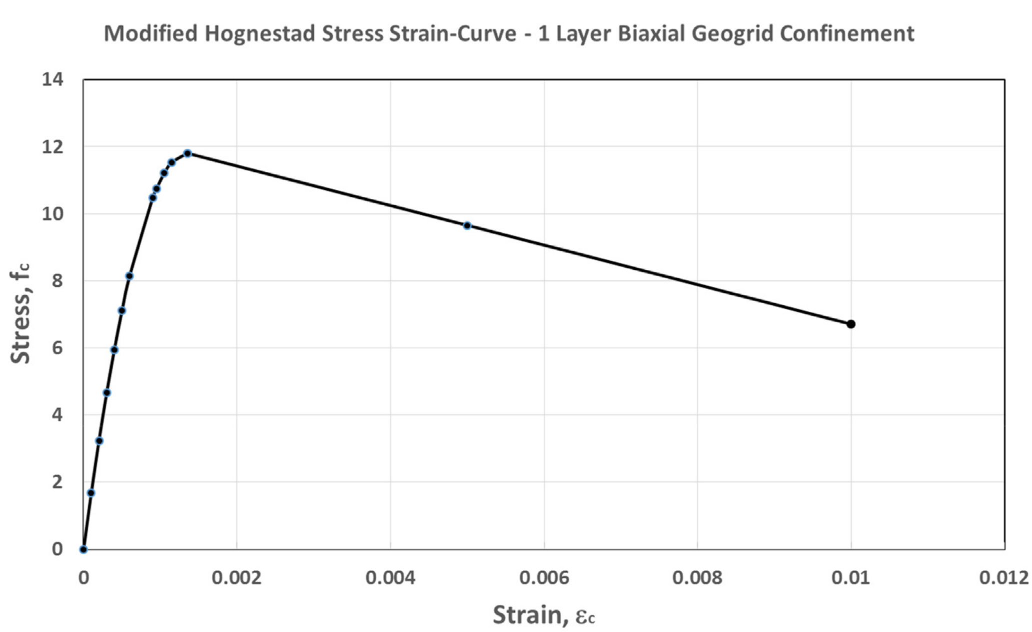

References

[1] M. Abdesssemed, S. Kenai, A. Bali, Experimental and numerical analysis of the behavior of an airport pavement reinforced by geogrids, Constr. Build. Mater. 94 (2015) 547–554.

[2] ACI 211.1-91. Standard practice for selecting proportions for normal, heavyweight, and mass concrete. ACI Committee 211, American Concrete Institute, Farmington Hills, Michigan; Reapproved 2009.

[3] A.S. Al-Hedad, E. Bambridge, M.N. Hadi, Influence of geogrid on the drying shrinkage performance of concrete pavements, Constr. Build. Mater. 146 (2017) 165–174.

[4] Al-Ayash Z, Kahil SN, Karakashian A, Mrad M, Chehab G, Saad G. Application of existing numerical models for prediction of geogrid confinement effectiveness of PCC columns. Proceedings of the Geosynthetics Conference, Portland, Oregon; 2015.

[5] Al-Qadi IL, Morian DA, Stoffels SM, Elseifi M, Chehab G, Stark T. Synthesis on use of geosynthetics in pavements and development of a roadmap to geosynthetically-modified pavements. Federal Highway Administration (FHWA) Report; 2008.

[6] G. Campione, N. Miraglia, Strength and strain capacities of concrete compression members reinforced with FRP, Cem. Concr. Compos. 25 (1) (2003) 31–41.

[7] R.S. Chidambaram, P. Agarwal, The confining effect of geo-grid on the mechanical properties of concrete specimens with steel fiber under compression and flexure, Constr. Build. Mater. 71 (2014) 628–637.

[8] R.S. Chidambaram, P. Agarwal, Performance evaluation of geogrid-confined beam-column joints with steel fiber reinforced concrete under cyclic loading, J. Test. Eval. 44 (1) (2015) 582–598.

[9] R.S. Chidambaram, P. Agarwal, Flexural and shear behavior of geo-grid confined RC beams with steel fiber reinforced concrete, Constr. Build. Mater. 78 (2015) 271–280.

[10] R.S. Chidambaram, P. Agarwal, Shear resistance behavior of geogrid-confined RC elements under static and cyclic loading, Curr. Sci. 117 (2) (2019) 260–271.

[11] F. El Meski, G. Chehab, Flexural behavior of concrete beams reinforced with different types of geogrids, J. Mater. Civ. Eng. 26 (8) (2014).

[12] A.Z. Fam, S.H. Rizkalla, Behavior of axially loaded concrete-filled circular fiber-reinforced polymer tubes, ACI Struct. J. 98 (3) (2001) 451–461.

[13] M.N.S. Hadi, Behaviour of FRP wrapped normal strength concrete columns under eccentric loading, Compos. Struct. J. 72 (4) (2006) 503–511.

[14] H. Itani, G. Saad, G. Chehab, The use of geogrid reinforcement for enhancing the performance of concrete overlays: an experimental and numerical assessment, Constr. Build. Mater. 124 (2016) 826–837.

[15] A. Khodaii, S. Fallah, F.M. Nejad, Effects of geosynthetics on reduction of reflection cracking in asphalt overlays, Geotext. Geomembr. 27 (1) (2009) 1–8.

[16] L. Lam, J.G. Teng, Design-oriented stress-strain model for FRP-confined concrete, Constr. Build. Mater. 17 (6) (2003) 471–489.

[17] J. Li, M.N.S. Hadi, Behavior of externally confined high-strength concrete columns under eccentric loading, Compos. Struct. J. 62 (1) (2003) 145–153.

[18] H.I. Ling, L. Zheng, Performance of geosynthetic-reinforced asphalt pavements, J. Geotech. Geoenviron. Eng. 127 (2) (2001) 177–184.

[19] J.B. Mander, M.J.N. Priestly, R. Park, Theoretical stress-strain model for confined concrete, ASCE J. Struct. Eng. 114 (8) (1988) 1804–1826.

[20] Maxwell, S. Effectiveness of geosynthetics in stabilizing soft subgrades. Project Report, Wisconsin Highway Research Program; 2005

[21] E.M. Palmeira, Advances in geosynthetics materials and applications for soil reinforcement and environmental protection works, Electron. J. Geotech. Eng. 13 (2008) 1–38.
[22] R. Park, T. Paulay, Reinforced Concrete Structures, John Wiley & Sons, New York - London - Sydney - Toronto, 1975.
[23] M.J.N. Priestly, F. Seible, E.R. Fyfe, Seismic Design and Retrofit of Bridges, Wiley, New York, 1996.
[24] S. Sivakamasundari, A.J. Daniel, A. Kumar, Study on flexural behavior of steel fiber RC beams confined with biaxial geogrid, Procedia Eng. 173 (2017) 1431–1438.
[25] Tang X, Kim S, Chehab G. Laboratory study of geogrid reinforcement in Portland cement concrete. Proceedings of 6th RILEM International Conference on Cracking in Pavements, Chicago, Illinois; pp 769-778, 2008.
[26] J.K. Wight, J.G. Macgregor, Reinforced Concrete: Mechanics and Design, Pearson Education Limited, Harlow, 2016.
[27] H. Yalciner, A. Kumbasarog, E. Ahmet, I. Turin, Confinement effect of geo-grid and conventional shear reinforcement bars subjected to corrosion, Structures 13 (2018) 139–152.